HiSST: International Conference on
High-Speed Vehicle Science Technology
26–29 November 2018, Moscow, Russia

Investigation of the Influence of the Perforated Walls of the T-128 Wind Tunnel on the Aerodynamic Characteristics of the Reentry Vehicle at Transonic Speed

S. A. Glazkov[1], A. R. Gorbushin[2], A. V. Semenov[3], A. V. Ledovsky[4], G. A. Trashkov[5]

Abstract

The paper is devoted to the study of the influence of wind tunnel perforated walls on the aerodynamic characteristics of the reentry vehicle model at transonic speed. An experimental investigations were carried out with model at zero angle of attack in the TsAGI transonic wind tunnel T-128 within the range of Mach number M=0.9-1.1 at various porosity values of test section walls F=2%; 6%; 10%. Aerodynamic forces and moments, acting on the model, were measured by 6-component internal strain gauge balance. A distribution of static pressure on the model surface and on test section perforated walls was measured along with static pressure fluctuations on the model. Parameters of the boundary layer on the perforated wall were measured by means of the rake with total pressure probes. Numerical investigations of the flow around the model in test section were performed by solving Reynolds Averaged Navier-Stocks (RANS) equations using Electronic Wind Tunnel software (EWT-TsAGI). Satisfactory agreement was obtained between the computational and experimental data on the influence of the test section perforated walls on the aerodynamic characteristics of the model and the flow parameters on the wall. The influence of the perforation coefficient on the model drag coefficient in the calculations and in the experiment turned out to be the same.

Key words: *perforated wall interference, transonic wind tunnel, perforation, reentry vehicle*

Nomenclature

C_D – drag coefficient
CFD – computational fluid dynamics
EWT – Electronic Wind Tunnel
F - perforation ratio
M – Mach number
PSD – power spectrum density
RANS – Reynolds Averaged Navier-Stocks equations
URANS – unsteady RANS
Q – dynamic pressure
R – coefficient in Darcy-type boundary condition
f – frequency
δ^* – displacement thickness
σ – standard deviation

[1] *Central Aerohydrodynamic Institute (TsAGI), 1, Zhukovsky st., Zhukovsky, Moscow reg., 140180, Russia, E-mail glazkov@tsagi.ru*
[2] *Central Aerohydrodynamic Institute (TsAGI), 1, Zhukovsky st., Zhukovsky, Moscow reg., 140180, Russia, E-mail gorbushin@tsagi.ru*
[3] *Central Aerohydrodynamic Institute (TsAGI), 1, Zhukovsky st., Zhukovsky, Moscow reg., 140180, Russia, д.1, E-mail aleksandr.semenov@tsagi.ru*
[4] *Central Aerohydrodynamic Institute (TsAGI), 1, Zhukovsky st., Zhukovsky, Moscow reg., 140180, Russia, E-mail avledovsky@gmail.com*
[5] *S.P. Korolev Rocket and Space Corporation "Energia", 4A, Lenin st., Korolev city, Moscow reg., 141070, Russia, E-mail gtrashkov@yandex.ru*

1. Introduction

The first experimental investigations of the wall interference effect in wind tunnels were carried out by D.P. Ryabushinsky [1]. He studied the influence of solid and open wind tunnel walls on the drag coefficient of a disk mounted perpendicular to the flow. The article [2] can be referred to the first works on the development of analytical methods for solving the boundary effect problem. A review of the further development of the methods for solving this problem is presented in [3]. The most difficult problem is the test section wall interference at transonic speeds, when the perturbations generated by the test model in the form of compression and expansion shock waves reach the flow boundaries, reflect from them, interact with each other, and return to the model.

The application of numerical methods in the experimental investigation technology in the wind tunnels of TsAGI at transonic speeds began in the 1980s due to the need to increase the reliability of aerodynamic characteristics of the Buran-Energia aerospace system models [4]. The combination of numerical integration of the Euler equations for infinite flow and the technical solution of sectional regulation of perforation in the T-128 wind tunnel made it possible to develop a technology for adapting perforated boundaries [5], which has been applied since 1986. Since 1996, methods based on numerical solutions of the Euler equations with boundary conditions on the test section perforated walls have been used to account for the boundary effect at transonic speed. The EWT-TsAGI software package was created in TsAGI [6]. The boundary conditions on the perforated walls were represented in the form of Darcy's law (linear relationship between the normal and longitudinal perturbation velocity components) and were determined experimentally [7].

Later, a module for the numerical solution of the RANS equations was added to the EWT-TsAGI software package. Currently, the program allows to solve numerically steady-state (RANS) and unsteady-state (URANS) equations, the possibility of large eddy simulation (LES) is realized.

This article is devoted to the experimental and computational investigations of the influence of perforated walls on the basis of the results of the reentry vehicle model testing in the T-128 wind tunnel. The computations were performed using the EWT-TsAGI software package.

2. Experimental investigations

2.1. Reentry vehicle model

The test model (Fig. 1) is a classical model of a segment-conical form. The peculiarity of the models of this type, to which reentry vehicles belong, is a low aspect ratio and a blunt nose. On the surface of the model, there are 48 pressure orifices with a diameter of 0.6 mm for measuring static pressure and 10 ports for measuring pressure fluctuations (Fig. 1a). The position of the static pressure ports provides pressure values along 3 longitudinal lines and, additionally, on the conical lateral surface area for a more detailed study of the separation zone and flow pattern change.

The static pressure is measured by a small-sized pressure module [8] installed in the model. Fluctuating pressures are measured using Kulite sensors of the XT-140 type. Two sensors are located on the frontal surface of the model, 3 - along a longitudinal line, 2 - on the bottom flat surface and 3 sensors - along the perimeter of on the maximum diameter of the conical surface.

The model is mounted on the rear sting whose diameter is chosen to be minimal (0.041 m), but providing the required strength. The rear sting was fixed in the wind tunnel sting support at an angle of 28° (Fig. 1b).

2.2. T-128 transonic wind tunnel

The T-128 wind tunnel is a variable-density continuous closed circuit wind tunnel [9]. The test section, where a model and the mixing chamber are located, is made in the form of one structural unit, which is usually called a changeable test section. The length of the test section is 12 m. The

inlet cross-sectional area is 2.75 m×2.75 m, the outlet cross-sectional area is 2.75 m×3.5 m. The T-128 is equipped with 4 interchangeable test sections.

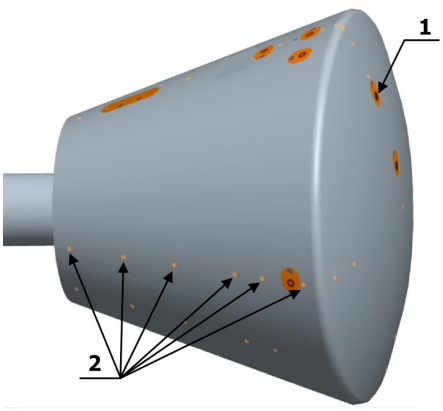

1 – unsteady pressure port P2,
2 – static pressure ports

a)

b)

Fig.1 Re-entry vehicle model
a) model general view; b) photo of the model in test section No. 1 of the T-128 wind tunnel

Test section No. 1 (Fig. 1b) is designed to investigate the aircraft models mounted on the sting supports of various types in the flow velocity range from M=0.15 to M=1.4. The sting support is fixed in a crescent-shaped rigid strut, which, in turn, is fixed to its drive mechanism. The pitch angle range of the mechanism is ±30°, and the yaw angle range is ±15°. Test section No. 1 has a sectionally-adjustable perforation. In total, there are 128 adjustable sections on the walls. The perforation is made in the form of circular stepped holes with a diameter of 24 mm and 20 mm, sectioned along the length and width of the test section walls. The perforation ratio opening coefficient (hereinafter for brevity, the perforation coefficient) of each section is adjustable in the range from F=0% to F=18%. Along the axial lines of the four test section walls, as well as the upper and lower walls of the nozzle, there are holes for measuring static pressure.

Structure and the main technical parameters of T-128 measuring system, which was used during the experimental studies, are given in paper [8].

2.3. Measuring of static pressure on the model surface and on the test section walls

Kulite differential piezoresistive transducers were used to measure the pressure pulsations. The transducers signals were converted and recorded by MIC-355M equipment (MERA Research & Production Company production) and MX-340.v6 modules installed on it. Ten pressure pulses transducers were installed on the reentry vehicle model. To estimate the incoming flow background noise characteristics, the static pressure pulsations were measured in test section on its perforated side wall axis at 1.715 m to test section entry. The XCS-062-5D Kulite transducer was used with ±0.35 bar pressure range. The signals recording was made at 54 kHz sampling frequency at 16 bit resolution. One regime recording duration was from 3 to 7 s.

2.4. Measuring of boundary layer parameters on the test section wall

The boundary layer parameters were measured by total pressure rake, which was mounted on the test section top wall at 5.583 m to its entry (Fig. 1b, top right area). Twenty-five transducers were installed on 200 mm rake. The rake is downstream from model in order the shock wave, generated by rake, not affect the model streamline. Thus, the shock wave which was formed at the model reached the boundary layer on the test section wall at a small distance before the rake at M>1 and distorted it. Due to this, the boundary layer parameters are studied in this paper under M≤1 only.
Fig. 2 shows the M number influence on the boundary layer velocity profile on a perforated wall for two perforation ratios. Under low perforation ratio, F=3÷6%, the growth of M number results into the slight increase of pattern fullness (see Fig. 2a). For higher values of F=10% this effect becomes more demonstrable (Fig. 2b).

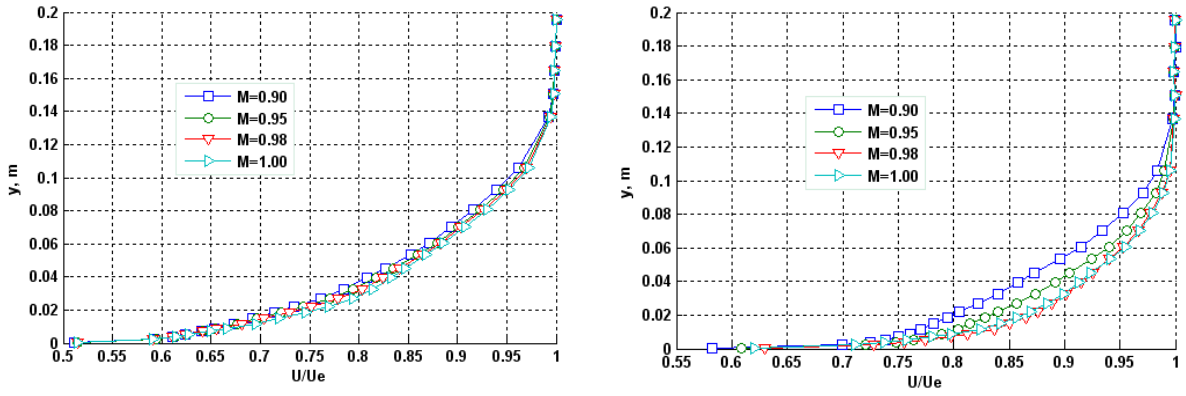

Fig.2 M number influence on speed profile in boundary layer on the test section wall
a) perforation ratio is F=3%; b) perforation ratio is F=10%

The increase of perforation ratio from F=3% up to F=10% leads the velocity profile to essential fullness increase (Fig. 2) and almost double lowering of boundary layer displacement thickness (Fig. 3). The displacement thickness decreases as the M number grows in transonic range. If perforation ratio is F=3% this decrease is ~10% under growth of M number from 0.9 up to 1.0, then, for F=10% it reaches ~30% already (Fig. 3).

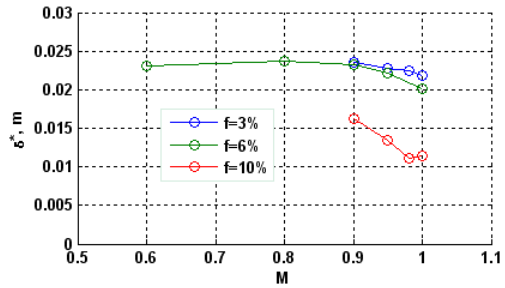

Fig.3 Perforation influence upon boundary layer displacement thickness on test section wall

The displacement thickness at the end of perforated zone is in 0.01÷0.024 m range (Fig. 3). This makes 0.7÷1.7% of half-height of test section. Such a low value of displacement thickness has allowed to transfer Darcy's boundary condition into the plane of test section wall for the problem of the numerical solution of RANS equations.

2.5. Measuring of aerodynamic loads by strain-gauge balance

The aerodynamic loads that act on re-entry vehicle model, were measured by six-component strain-gauge balance, which were manufactured particularly for this model. The axial force range of balance was 5 kN and the accuracy was 3 N. For typical test regimes with average dynamic pressure of Q~37 kPa, the accuracy of the drag coefficient is ΔC_D~0.002. The loads measurement results are corrected considering the balance temperature effect [10], model and balance metric part weights [11].

3. Computational investigations

3.1. Brief description of EWT-TsAGI software

The EWT-TsAGI package allows solving numerically Euler equations, the stationary (RANS) and unsteady (URANS) Navier-Stocks equations using the Reynolds-averaging. The possibility is implemented for large eddy simulation (LES). The special initial and boundary conditions are previewed such as the wind tunnel starting, permeable walls (perforated and slotted), moving belt, plenum chamber. The blocked grid template with the special block for model is created. The supporting devices are separated into a special block. The algorithm is developed to reshape the grid at variation of α- and β-angles.

The EWT-TsAGI program makes it possible to solve three main tasks, which the experimentalists of TsAGI confronted with:

- Consideration of the main systematic errors of experiment, i.e. the influence of flow boundary and supporting devices (various types of stings for full models [12], peniche for half models [13], slotted wall interference [14]), influence of wind tunnel turbulence;
- Minimization of perforated walls influence in the transonic velocities range by perforation adaptation technology [15];
- Design of aerodynamic contours of supporting devices and test section perforated walls that create the minimum flow disturbances in model location area [4].

3.2. Experimental and computational research program

The aim of experiments was the investigation of wall perforation effect on the reentry model drag, wall boundary layer parameters, steady and unsteady static pressure on the model and test section walls at transonic speed. Experimental studies of the perforation influence were carried out in the range of Mach number M=0.9-1.1. In this case, the range of the Re number, based the model diameter, was Re=2.5–2.8 million. The tests were carried out at three values of the perforation ratio: F=3; 6; 10%. The distance from the beginning of the test section to the forebody of the model was 4.606 m. The test section blockage (the ratio of the model midsection area to the test section cross-section area) was 0.52%.

The aim of CFD work was the verification of computational model applied to the transonic flow over the reentry vehicle model in test section with perforated walls. The calculations of the flow around a model in the tunnel were performed by numerical solution of the RANS equations using the EWT TsAGI software package for Mach number range M=0.9-1.2. The SA turbulence model and implicit Godunov-Kolgan-Rodionov scheme were used for solving the Reynolds equations. The thickness of the cell closest to the model surface was 3×10^{-7} m to resolve boundary layer on the model. The computational domain was divided into 30 blocks and structured grid comprised in total nearly 2 mln cells. All of the calculations were performed with the model geometry together with a forward part of the sting up to a crank at zero angle of attack. To simulate the flow in the test section of the T-128 wind tunnel, a duct of square cross section with a side of 2.75 m and 20 m long was chosen. The nose of the model is located at a distance of 10 m from the duct forepart. The computational region, taking into account the symmetry of the flow, comprises a 1/8 part of the duct. The Darcy condition was set on the permeable walls. The constant R values were used in Darcy condition regardless of flow direction across the perforation in order to simplify the calculation model.

4. Results

4.1. Static pressure pulsations

Statistical processing of the initial experimental data was carried out using known methods of digital analysis of random time processes [16].

The standard processing procedure is as follows. For each sensor, the realization parts corresponding to the time intervals for recording aerodynamic characteristics and flow parameters at selected modes are allocated. The realization for each measuring channel is divided into a set of shortened non-overlapping realizations with the duration of, for example, $T_N \approx 76$ ms (N=4096 samples at the data acquisition frequency f=54 kHz). On each shortened realization, the average value is determined and its centering (elimination of the mean value) is performed.

The unbiased estimate of the dispersion of the n^{th} shortened centered realization is calculated as follows:

$$\sigma_n^2 = \sigma^2\left(t_j\right) = \frac{1}{N-1}\sum_{k=1}^{N} x_k^2 , \quad t_j = t_0 + j\frac{N}{2}\Delta t ,$$

and the average deviation σ_{xx}^2 during the whole realization is determined by averaging over the ensemble of shortened realizations, the number of which were 92 with a measurement duration of 7 seconds and a sampling frequency of 54 kHz. The corresponding root-mean-square deviation of the

process σ from the mean value is determined as the square root of deviation value, and the one-way spectral power density normalized to the mean square of the pressure pulsations:

$$PSD = \frac{G_{xx}(f_k)}{\sigma_{xx}^2 \Delta f} \ [c],$$

where

$$G_{xx}(f_k) = \frac{2}{m} \sum_{i=1}^{m} \left[X_i^*(f_k) X_i(f_k) \right], \quad k = 0, 1, \ldots N/2 \ ;$$

$$X(f_k) = \frac{1}{N} \sum_{n=1}^{N} x_n e^{-i2\pi(k-1)(n-1)/N}, \quad x_n = x(t_n)$$

Spectral analysis using the fast-Fourier-transform algorithm was performed in the frequency range of 13.5 Hz<f<27 kHz in the bands of constant width Δf≈13.5 Hz with the length of the shortened realization of 4096 samples. Thus, the relative errors of statistical estimates are $[G_{xx}] \approx 1/\sqrt{m}$ ~0.104.

The influence of the Mach number and the perforation coefficient on the standard deviation (SD) of the static pressure coefficient 6/Q is shown in Fig. 4a for pressure port P2 on the forward part of the model and on Fig. 4b on test section wall. The level of pulsations at M=0.9 on the model is 35% less than on the test section wall. With increasing Mach number to M=1.1 this difference is leveled off. A change of the perforation ratio from F=3% to F=6% practically does not affect the SD of the static pressure coefficient pulsations, both on the model (Fig. 4a) and on the wall (Fig. 4b). At F=10%, the SD of the pressure pulsations on the model is approximately 10% lower than for F=3% or F=6% (Fig. 4a), while on the wall at F=10% the SD increases significantly and has a maximum at M=1.02 (Fig. 4b). The increased level of pulsations on the wall at F=10% is explained by the fact that a significant part of the pulsation energy is in the low-frequency region of spectrum in the range of 100-200 Hz (Fig. 5b). The noise level due to the perforation of the walls on the tunnel axis is less for a mean of 2-3 dB than on the walls of the test section. Strong low-frequency noise from perforation at the coefficient of 10% is reduced by 10 dB on the model. In the low-frequency region of the spectrum, f<700 Hz, the pulsation level on the model at F=10% is higher than at small values of the perforation coefficient, while in the middle spectrum region 3 kHz<f<9 kHz the ratio of the pulsation levels is inverse.

The noise caused by the flow around the model is concentrated in the lower spectrum region: f<2kHz, and this noise is not detected by the sensor located upstream on the wall of the WT.

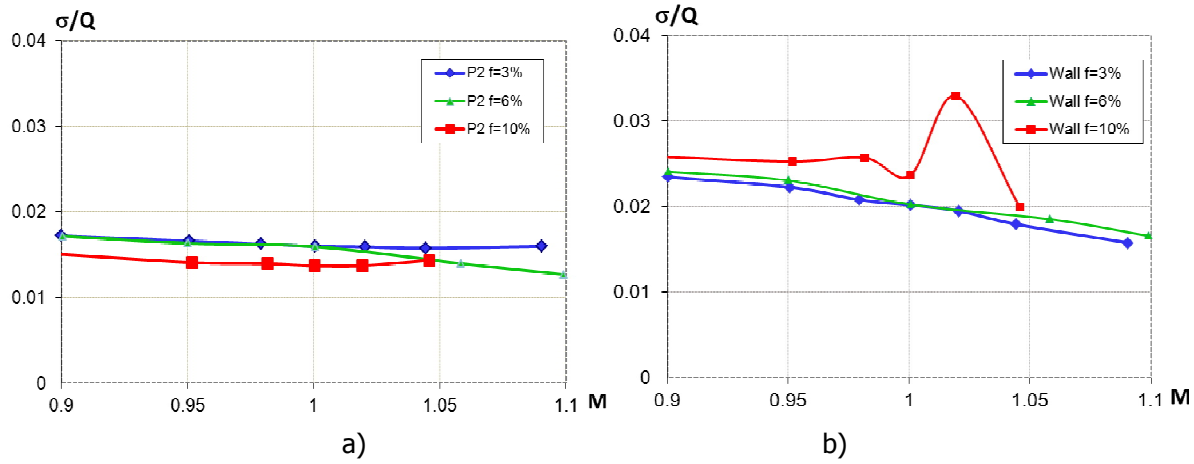

Fig 4. Influence of the Mach number and perforation on the standard deviation of the pressure coefficient
a) at point P2 on the model surface; b) on the test section wall

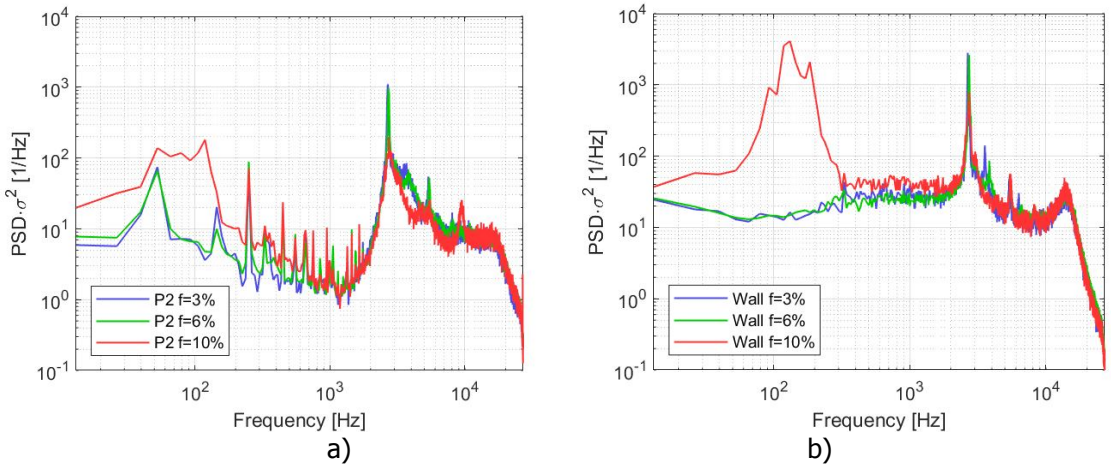

Fig 5. The power spectral density of pressure pulsations at M=1.0 and different perforation ratio a) at point P2 on the model surface; b) on the test section wall

For all values of the perforation coefficient in the spectrum of pulsations on the model and on the test section wall, a tone f~2.7 kHz due to perforation [9], as well as two multiple tones f~5.4; 8.1 kHz are presented. In the lower spectrum region, a tone f=332 Hz is observed, which appears on the rotating blades of the compressor [9].

4.2. Mach number distribution on the test section walls

The distribution of the Mach number on the test section wall of the T-128 is shown in Fig. 6 for two perforation ratio values F=3% and 6% when the Mach number of the incoming flow is about M≈1.05. The scaled model with sting and their position are also shown on both plots. In order for the conditions for comparing the calculation and experiment results to be the closest, the experimental data are taken from the lower wall of the test section. The ducted flow analyses were carried out within the framework of solving the RANS equations using the TsAGI EWT package. The permeability coefficients in the boundary condition on the perforated walls were chosen R=0.5 for the perforation coefficient F=3% and R=1.0 for F=6% [7].

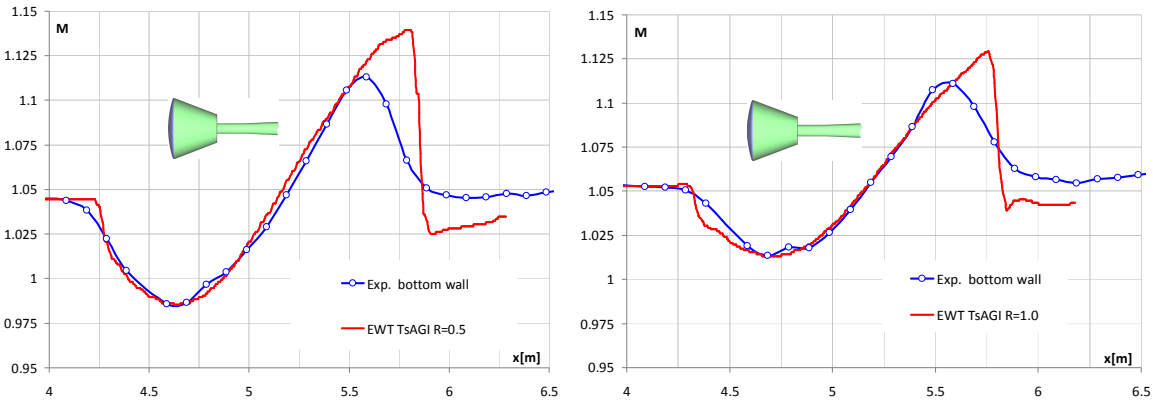

Fig 6. Mach number distribution on the test section wall a) M=1.044, F=3%; b) M=1.054, F=6%

Satisfactory agreement between the calculated and experimental distributions of the Mach number on the wall takes place right up to the impact point of the closing shock wave (up to the maximum Mach number) for both values of the perforation coefficient F. The difference between experimental and calculated data in the region of shock wave may be due to two reasons. The first one is the absence of viscous-inviscid interaction of the shock and boundary layer in computational model. The second one is associated with the simplified boundary condition with constant R value applied both for the inflow and outflow from test section. In fact there is a difference in R values for inflow and outflow from test section, as it was shown in [7].

Amplitude of Mach number perturbation on the wall is higher at F=3% both for CFD and experimental results than at F=6%.

Figure 7 presents calculated distribution of Mach number in the plane of symmetry at M=1.044 and R=0.5 corresponding to the case shown in Fig. 6a. CFD results shows a complicated flow over the model with a large separation region, wide wake and the shock wave reaching the perforated wall. Wall interference at transonic speed is characterized by interaction of shock and expansion waves originated on the model with perforated walls of test section and subsonic model wake.

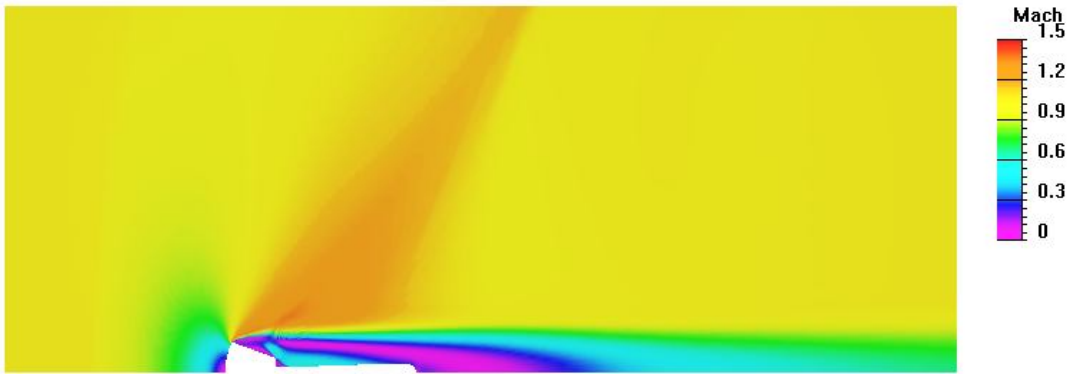

Fig 7. Mach number distribution in the plane of symmetry, M=1.044, R=0.5

4.3. Model drag

The influence of the perforation coefficient of the walls on the drag coefficient of the reentry vehicle model, obtained in experimental and computational studies, is shown in Fig. 8.

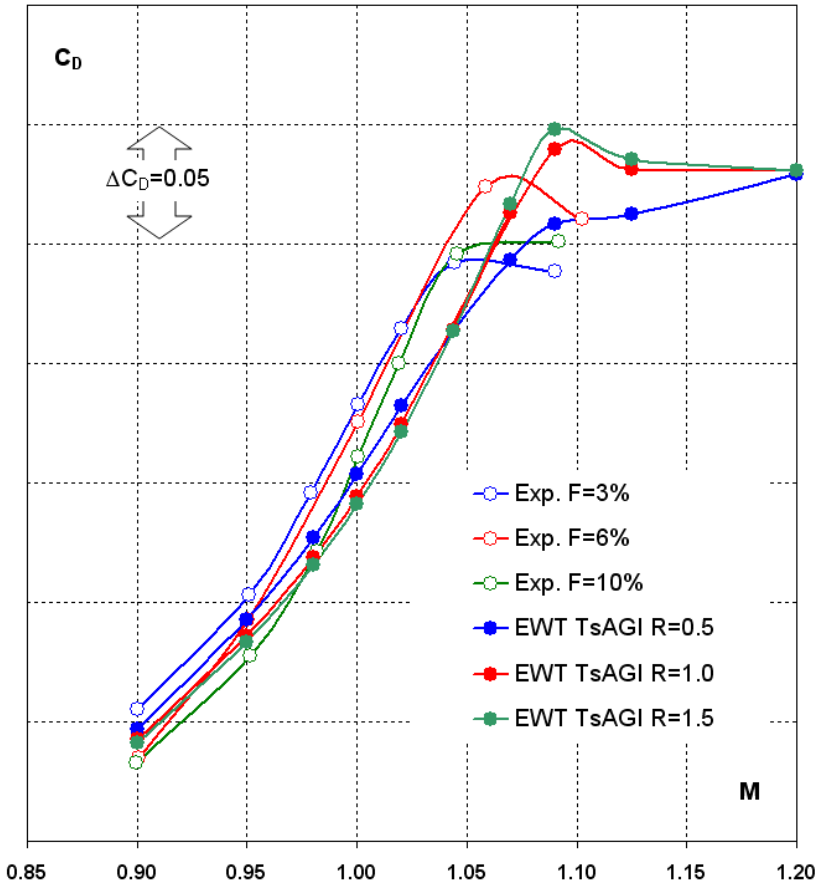

Fig 8. Influence of the perforation coefficient on the drag coefficient of the model

The maximum difference of the drag coefficient values when changing the perforation coefficient in the range of F=3-10% is observed in the experiment at M=1.06 and is 0.03. For the remaining values

of M, it does not exceed 0.02. Such a difference may be considered as not a great value taking into account a large separation region at the rear part of the model. In the range of M≤1.02 the model has higher drag when F=3% while at M>1.02 larger drag takes place at F=6%. Maximum drag takes place in experiment in Mach number range 1.05<M<1.1.

Computational results for all perforation ratios are close to each other up to M=1.04 (ΔC_D<0.005). The maximum difference of the drag coefficient values when changing the perforation coefficient in the range of F=3-10% is observed in computations at M=1.09 and is 0.04. Wall interference effect on model drag disappeared at M≥1.2 when the shocks reflected from perforated wall interact with the model wake fare from the model. Drag coefficient for F=3% is higher than for other perforation ratios both for CFD and experimental results up to M<1.04 and lower for higher Mach numbers.

Experimental and CFD drag coefficients are quite close at M=0.9. The slope of CFD results is slightly lower than that of experimental ones. Maximum CFD drag coefficient value takes place in Mach number range 1.09<M<1.2. The influence of the perforation coefficient on the model drag coefficient in the calculations and in the experiment turned out to be the same. One of the possible explanations of the difference between experimental and calculated data may be attributed to the simplified sting geometry used in calculations. It would be helpful to investigate the influence of different R values for inflow and outflow from test section on the interference of shock and expansion waves with model wake, and consequently model drag.

5. Conclusion

The experimental investigation of the flow around the reentry vehicle model at a zero angle of attack in the T-128 wind tunnel of TsAGI in the transonic speed range M=0.9-1.1 with three values of the perforation coefficient of the test section walls F=3%, 6%, 10% was carried out.

Measurements of the boundary layer parameters on the test section wall showed that the displacement thickness at the end of the perforated area is 0.7-1.7% of the test section half-height, which allows using the boundary condition of the Darcy type in the wall plane in the numerical solution of the RANS equations.

The minimum level of pulsations on the model occurs at F=10%. The noise level caused by the perforated walls along the tunnel axis is on average 2-3 dB less than on the test section walls. In the low-frequency region of the spectrum, f<700 Hz, the level of pulsations on the model at F=10% is higher than at small values of the perforation coefficient, while in the middle part of the spectrum 3 kHz<f<9 kHz, the ratio of pulsations is the opposite.

Satisfactory agreement was achieved between the calculated and experimental distributions of the Mach number on the wall up to the position of the closing shock wave. One of the possible explanations of the difference between experimental and calculated data in the region of shock wave is the absence of viscous-inviscid interaction of the shock and boundary layer in computational model.

The influence of the perforation coefficient on the model drag coefficient in the calculations and in the experiment turned out to be the same.

A new set of calculations with real sting geometry is required to understand the difference in drag coefficient slope and the discrepancy between CFD and experimental data at M>1.04.

References

1. Gorbushin, A.R.: Pioneering Russian wind tunnels and first experimental investigations, 1871–1915. Progress in Aerospace Sciences 95C, 99-139 (2017). https://doi.org/10.1016/j.paerosci.2017.10.003
2. Theodorsen, T.: The Theory of Wind-Tunnel Wall Interference. NACA TR-410, (1932)
3. Glazkov, S.A., Gorbushin, A.R., Ivanov, A.I., Semenov, A.V.: Recent experience in improving the accuracy of wall interference corrections in TsAGI T-128 wind tunnel. Progress in Aerospace Sciences, Vol. 37, No 3, (2001)

4. Chernyshev, S.L., Neyland, V.Ya., Bosnyakov, S.M., Glazkov, S. A., Gorbushin, A.R., Kursakov, I.A., Vlasenko V.V.: Experience in the application of numerical methods to TsAGI's wind-tunnel testing techniques, 5th Symposium on Integrating CFD and Experiments in Aerodynamics, JAXA, Tokyo, (2012)
5. Neyland, V.M., Ivanov, A.I., Semenov, A.V., Semenova, O.K., Amirjanz, G.A.: Adaptive-Wall Perforated Test Section for Transonic Wind Tunnels. AGARD-CP-585, 1997.
6. Neyland, V., Bosniakov, S., Glazkov, S., Ivanov, A., Matyash, S., Mikhailov, S., Vlasenko, V.: Conception of electronic wind tunnel and first results of its implementation. Progress in Aerospace Sciences, Vol. 37, No 2, pp. 121-145 (2001)
7. Glazkov, S.A., Gorbushin, A.R., Semenov, A.V.: Experimental study of boundary conditions on the perforated walls of test sections no. 1 and 2 of T-128 transonic wind tunnel. AIP Conference Proceedings 2027, 040025 (2018); https://doi.org/10.1063/1.5065299
8. Burov, V.V., Volobuev, V.S., Glazkov, S.A., Gorbushin, A.R., Chumachenko, E.K.: Measuring and Computational System of TsAGI T-128 Transonic Wind Tunnel. Autom Remote Control 72: 634 (2011). https://doi.org/10.1134/S0005117911030147
9. Biryukov, V., Glazkov, S., Gorbushin, A., Ivanov, A., & Semenov, A. (2005). Experimental investigation of the effect of nozzle shape and test section perforation on the stationary and non-stationary characteristics of flow field in the large transonic TsAGI T-128 Wind tunnel. The Aeronautical Journal (1968), 109(1092), 75-82. doi:10.1017/S0001924000000579
10. Bogdanov, V.V., Gorbushin, A.R., Volobuyev, V.S.: Research on thermal dynamics of strain-gauge balance and development of methods for its temperature error reduction. TsAGI Science Journal, v40, i5, p.619-629 (2009). DOI: 10.1615/TsAGISciJ.v40.i5.80
11. Gorbushin, A.R.: A method for taking into account the influence of the model and dynamometer weights on the strain-gauge balance readings. TsAGI Science Journal, v40, i4, p.485-495 (2009). DOI: 10.1615/TsAGISciJ.v40.i4.70
12. Glazkov, S.A., Gorbushin, A.R., and Kursakov, I.A.: Fin and rear stings support effects on the flow around the aircraft model. In 29th Congress of the International Council of the Aeronautical Sciences, ICAS 2014
13. Glazkov, S.A., Gorbushin, A.R., Kursakov, I.A., Jasenok, K.A.: Investigation of peniche and wall interference on half-model using CFD. AIP Conference Proceedings 1770, 030010 (2016). http://dx.doi.org/10.1063/1.4963952
14. Kursakov, I.A., Gorbushin, A.R., Bosnyakov, S.M. et al. CEAS Aeronaut J (2018) 9: 319. https://doi.org/10.1007/s13272-017-0248-1
15. Glazkov, S.A.: Parameter porosity of the perforated walls effect on amplitude of the reflected disturbance in location of model for supersonic flows. TsAGI Science Journal, v49, i6, p.53-63, (2018). DOI: 10.1615/TsAGISciJ.2018029193
16. Bendat, J.S., Piersol, A.G.: Measurement and Analysis of Random Data. Julius S. John Wiley & Sons, New York – London – Sydney (1967)

